PCCP

Ultrafast relaxation dynamics of electronically excited piperidine: Ionization signatures of Rydberg/valence evolution

Journal:	*Physical Chemistry Chemical Physics*
Manuscript ID	CP-ART-06-2016-004494.R1
Article Type:	Paper
Date Submitted by the Author:	08-Aug-2016

Complete List of Authors:	Klein, Liv; University of Copenhagen, Department of Chemistry Thompson, James; Heriot-Watt University, Institute of Photonics & Quantum Sciences Crane, Stuart; Heriot-Watt University, Institute of Photonics & Quantum Sciences Saalbach, Lisa; Heriot-Watt University, Institute of Photonics & Quantum Sciences Sølling, Theis; University of Copenhagen, Department of Chemistry Paterson, Martin; Heriot-Watt University, Institute Of Chemical Sciences Townsend, David; David Brewster Building, School of EPS - Physics

Ultrafast relaxation dynamics of electronically excited piperidine: Ionization signatures of Rydberg/valence evolution

Liv B. Klein[1,†], James O. F. Thompson[2,†], Stuart W. Crane[2], Lisa Saalbach[2], Theis I. Sølling[1], Martin J. Paterson[3] and Dave Townsend[2,3,*]

[1] *Department of Chemistry, University of Copenhagen, Universitetsparken 5, DK-2100 Copenhagen Ø, Denmark*

[2] *Institute of Photonics & Quantum Sciences, Heriot-Watt University, Edinburgh, EH14 4AS, United Kingdom*

[3] *Institute of Chemical Sciences, Heriot-Watt University, Edinburgh, EH14 4AS, United Kingdom*

Abstract

We have investigated the electronic relaxation dynamics of gas-phase piperidine (a secondary aliphatic amine) using time-resolved photoelectron imaging. Following 200 nm excitation, spectrally sharp and highly anisotropic photoelectron data reveal ultrafast (60 fs) internal conversion between the initially excited $3p_x$ Rydberg state and the lower-lying 3s Rydberg state, mediated by the evolution of nσ* valence character along the $3p_x$ N-C bond. This behaviour is in good agreement with previously reported findings for several tertiary aliphatic amines. In contrast to the these systems, however, much broader photoelectron signals exhibiting only very small angular anisotropy and two distinct decay timescales (180 fs and 1.7 ps) were also observed. As confirmed by our supporting calculations, this is attributable to nσ* valence character now evolving along the N-H stretching coordinate within the 3s Rydberg state as the molecule starts dissociating to yield H atom photoproducts in conjunction with ground state piperidinyl radicals. By analogy with systems such as ammonia and morpholine, we conclude this event may occur either promptly or, alternatively, via a "frustrated" process where the system repeatedly traverses the upper cone of a conical intersection with the ground state until the required region of phase space is sampled to facilitate non-adiabatic population transfer. Our findings reveal the role of several different nuclear coordinate motions in driving stepwise internal conversion across multiple potential energy surfaces and the distinct photoionization signatures that are associated with these processes.

* Corresponding author. E-mail: d.townsend@hw.ac.uk

† These authors contributed equally to this work.

I. INTRODUCTION

The amine functional group is extremely common in a wide range of compounds occurring in organic chemistry and in nature, appearing, for example, in the DNA bases, amino acids and neurotransmitters. It is also a very simple chromophore, which absorbs ultraviolet (UV) light by excitation of the lone pair electron on the nitrogen atom. Since amine groups are active in a variety of photochemical environments, this leads to an interest in determining the basic influence of the structure around the nitrogen chromophore on the overall photodynamics of the system.

We have recently reported detailed investigations of non-adiabatic relaxation dynamics in several tertiary aliphatic amines using time-resolved photoelectron imaging (TRPEI) in conjunction with supporting quantum-chemistry calculations.[1, 2] In all cases, it was concluded that a member of the 3p Rydberg manifold develops increasing nσ* valence character as N-C bond lengths are extended and that this plays a primary role in mediating various internal conversion processes within these systems following UV excitation at 200 nm. Additionally, we saw no experimental or theoretical evidence of similar mixed Rydberg/valence behaviour in the energetically lower-lying 3s state. As such, direct N-C bond fission within this state does not appear to be a facile channel in these systems as they are strongly bound along this coordinate of their potential energy surfaces. Based upon several independent pieces of evidence (temporal evolution of photoelectron angular distributions, state mixing calculations and the effect of reducing molecular symmetry), the ultimate fate of the 3s state instead appears to be a subsequent re-crossing back to a repulsive part of the 3p manifold following intramolecular vibrational redistribution on an extended timescale ranging from ~40 ps to >1 ns. This was a particularly striking result as the evolution of nσ* or πσ* character along N-X, O-X and S-X coordinates has now become well-established as a commonly occurring phenomenon in s-type Rydberg states of many small molecular species,

exerting significant influence on the excited state photochemistry.[3, 4] For the simplest amines ammonia and methylamine, 3s to nσ* evolution along the N-H bond leads to dissociative relaxation pathways producing H atom fission products following UV excitation (with CH_3 elimination also being observed at higher excitation energies in methylamine).[3] In ammonia, this decay pathway is reflected in the extremely short (sub-picosecond) excited state lifetimes that have been reported using time-resolved spectroscopic methods.[5-7] Dimethylamine has also been predicted to show similar photochemistry when excited to its first excited state ($3s \leftarrow n_N$),[8] with H atom photoproducts generated via quantum tunnelling of the hydrogen atom through a shallow barrier along the N-H coordinate.[9] Increasing the system complexity slightly more, the dissociation dynamics of trimethlylamine have been investigated experimentally following 193 nm excitation, with CH_3 elimination observed to the major dissociation pathway.[10] It is interesting to note, however, that time-resolved photoelectron spectroscopy measurements employing 200 nm excitation on this system have reported a relatively long (>>10 ps) 3s state lifetime (following sub-picosecond internal conversion from the initially prepared 3p manifold).[11] The much larger mass of the CH_3 group relative to that of an H atom suggests quantum tunnelling is unlikely to be a factor here. In addition, given the similarly long 3s state lifetime observed in numerous other tertiary amine species previously investigated by both ourselves[1, 2] and others[12-15] (all at excitation wavelengths close to 200 nm), it seem likely that equivalent dynamics operate in all these cases (i.e. CH_3 elimination does not occur directly along the N-C coordinate of the 3s state and the overall relaxation proceeds via an alternative mechanism).

On the basis of the work documented above, a clear trend in 3s state lifetimes (and associated decay mechanisms) appears to be emerging in amines following UV excitation: Primary and secondary species exhibit ultrafast (<1 ps) decay, mediated by the evolution of dissociative σ* valence character along the N-H bond of the 3s state. Tertiary systems, on the

other hand, exhibit excited state dynamics that are typically 1-2 orders of magnitude slower, partly as a consequence of the 3s state being bound along the analogous N-C coordinate. This situation appears to be complicated, however, when species other than *aliphatic* amines are considered. This is illustrated, for example, in our recent TRPEI measurements conducted on aniline and *N*,*N*-dimethylaniline (*N*,*N*-DMA) – primary and tertiary *aromatic* amines, respectively.[16] Here both systems were observed to exhibit 3s excited state lifetimes of <100 fs. As confirmed by supporting theory, this is a consequence of πσ* valence character evolving along the N-H (aniline) and N-CH_3 (*N*,*N*-DMA) bonds. In both systems, direct H or CH_3 elimination was found to be in competition with internal conversion to a lower-lying ππ* valence state. The introduction of such additional electronic states therefore appears to have a significant impact on the relaxation dynamics of amine systems. In some respects this is perhaps unsurprising, but such an observation clearly highlights the need for more expansive and systematic photochemical studies on this important class of molecules. In particular, the highly-differential time-, energy- and angle-resolved information provided by the TRPEI approach may potentially reveal a great deal of new mechanistic insight.

Here we report a new TRPEI study, supported by theoretical calculations, of the cyclic secondary amine piperidine following single-photon excitation at 200 nm and subsequent ionization using 267 nm (a 1+1′ scheme). This aliphatic system (shown in Fig. 1, along with its UV absorption spectrum) contains the same number of carbon atoms as several tertiary amines we have studied recently,[1] but clearly differs in having a hydrogen atom bonded directly to the nitrogen centre. Building on our previous work, a principal aim of this present study is to conduct a detailed investigation of TRPEI spectral signatures obtained for secondary amines that are free from the very broad and intense photoelectron bands associated with ππ* valence state ionization (such as those seen in aniline-based motifs). This potentially obscures the presence of weaker photoelectron features, complicating data analysis

in unsaturated species. Our findings will therefore provide a valuable benchmark for planned future studies investigating larger amine systems incorporating additional unsaturated chemical functionality. Although the excited state spectroscopy and dynamics of gas-phase piperidine has received only a small amount of attention[17-21], by analogy with other secondary aliphatic systems the excited state lifetimes should be extremely short (<1 ps). This appears to have been confirmed very recently by Zhang and co-workers[17], who have reported a TRPEI and time-resolved mass spectrometry study of piperidine using 400/800nm (2+2′) and (2+3′) multi-photon pump-probe ionization – the latter of which provides an equivalent total pump + probe energy to that used in our proposed (1+1′) approach. These authors report two ultrafast decay components with exponential time constants of 62 fs and 184 fs, interpreted simply as S_1 to S_2 and S_2 to S_0 internal conversion, respectively. We also highlight that Ashfold and co-workers have undertaken extensive H atom Rydberg tagging measurements on the related species morpholine (where the carbon sitting furthest from the nitrogen centre in the piperidine ring system is replaced with an oxygen atom).[22] At all selected excitation wavelengths spanning the 250-193 nm region, rapid N-H bond fission was inferred to be directly mediated by an electronic state exhibiting nσ* valence character. Two distinct H atom kinetic energy release channels were also observed, attributed to the production of concomitant ground state morpholinyl radicals formed either by (i) direct passage through a conical intersection (CI) connecting the nσ* and S_0 states or (ii) a more "frustrated" process where molecules repeatedly resample this CI until reaching the required geometry (planar about the N atom) for population transfer to occur.

II. EXPERIMENTAL METHODOLOGY

The experimental TRPEI setup has been described in detail elsewhere,[23] and is identical to that used in our recent study of several tertiary amine systems.[1] Briefly, piperidine (Sigma-Aldrich, 99%) was placed in an external bubbler maintained at 0 °C and introduced

into the source chamber of the photoelectron spectrometer using a helium carrier (1 bar). A 1 kHz pulsed valve (Ø=150 μm) was used to generate a molecular beam,[24] which passed into the main interaction chamber through a skimmer and was intersected at 90° by co-propagating pump and probe laser pulses. These were harmonics derived from the fundamental 800 nm output of a 1 kHz regeneratively amplified Ti:Sapphire laser system (Spectra-Physics, Spitfire Pro/Empower) seeded by a Ti:Sapphire oscillator (Spectra Physics, Tsunami/Millennia Pro). Thin β-barium borate crystals were used as the non-liner optical medium. A PC-controlled linear translation stage enabled precise control of the temporal delay between pump (200 nm, ~0.5 μJ/pulse) and probe (267 nm, ~2.0 μJ/pulse), which were then combined using a thin dichroic mirror and focussed into the spectrometer through a 2.0 mm thick CaF_2 window using a concave aluminium mirror (f = 50 cm). Resonant (1+1′) pump-probe ionization of piperidine seeded within the molecular beam occurred between the repeller and extractor electrodes of a magnetically shielded electrostatic lens set-up optimised for velocity-map imaging.[25] A CCD camera (640 × 480 pixels) then recorded the positions of photoelectrons striking a 40 mm dual micro-channel plate/P47 phosphor screen positioned at the end of a flight tube. Ion time-of-flight data, recorded before commencing photoelectron acquisition, confirmed no significant cluster formation in the molecular beam. TRPEI data collection sampled pump-probe delays Δt of -500 fs to +1000 fs in 50 fs steps and 9 exponentially increasing steps out to +10 ps. A typical data set comprised approximately 20 such scans and also included measurement of time-invariant pump-alone and probe-alone signals at each delay position (for subsequent background subtraction). A pump-probe cross-correlation of 160 ± 20 fs was obtained directly inside the spectrometer from non-resonant, two-colour (1 + 1′) multiphoton ionization of nitric oxide and three-photon, non-resonant 267 nm ionisation of xenon provided energy calibration data.

III. EXPERIMENTAL RESULTS

A. UV/VIS Spectrum

Prior to commencing TRPEI measurements, the UV vapour-phase absorption of piperidine at room-temperature was characterised using a commercial benchtop spectrometer (Fig. 1). The spectrum obtained exhibits a weak first absorption band (assigned to $3s \leftarrow n_N$ excitation) that is only partially resolved as a small shoulder on a more intense second band ($3p \leftarrow n_N$). Compared to spectra of tertiary aliphatic amines of similar size[1] the strong second band is noticeably blue-shifted, with a maximum at 198 nm. This is in accordance with earlier spectral observations and assignments for other amine systems[26-30] and is also in good overall agreement with our calculations (described in detail later and summarized in Table I). Key points of relevance here are (i) Fig. 1 shows no appreciable absorption at 267 nm, ensuring that the TRPEI data will be free from unwanted "probe-pump" signals evolving to negative time delays; (ii) 200 nm excitation will only populate 3p Rydberg states to any significant extent. More specifically, our oscillator strength calculations (Table I) show this will predominantly be to the lowest lying member of the manifold ($3p_x$).

B. Time-resolved Photoelectron Spectra

Photoelectron images resulting from (1 + 1′) piperidine ionization at selected pump-probe delay times are shown in Fig. 2. As for tertiary aliphatic amines excited at similar pump energies,[1] piperidine exhibits a pair of sharp, highly anisotropic ring features peaking along the laser polarization direction. In contrast to tertiary systems, however, the overall excited state dynamics appear significantly faster (by an order of magnitude or more) and the data clearly show an additional feature that is largely isotropic and extends broadly across the inner part of the images. The upper panel of Fig. 3 shows a time-resolved photoelectron spectrum generated from a full set of background-subtracted images. For ease of comparison with data previously reported for several other amine systems,[1, 2, 11-15] the energy axis is

plotted using excited state binding energy E_B, i.e. $E_B = E_{h\nu(probe)} - E_{(electron)}$. Fig. 4 shows the same spectrum from a "top-down" viewpoint with the intensity plotted on a natural logarithmic scale. No significant signal is observed at Rydberg binding energies <2.0 eV, which is in agreement with predictions based on the total pump + probe energy (10.85 eV) and the adiabatic D_0 ionization potential of 8.20 eV reported by Rozeboom and Houk.[31] The D_1 cation state is, in principle, just energetically accessible[31, 32] but no photoelectron signals obviously attributable to ionization into this state are observed. The narrow features seen in Fig. 4 centred at 2.55 eV and 3.35 eV (the latter of which appears to have a slightly delayed onset from zero pump-probe delay) correspond to the two sharp, anisotropic rings seen in the raw image data presented in Fig. 2. On the basis of our current calculations (detailed below), these may be attributed to ionization from states of $3p_x$ and 3s Rydberg character, respectively. In further support of this assignment, the narrow width of the peaks reflects a strong propensity for diagonal (i.e. $\Delta v = 0$) transitions to the cation and the pronounced anisotropy seen in the associated photoelectron angular distributions also suggests the excited states possess well-defined angular momentum. Both observations are strong indicators of Rydberg state ionization. The diagonal nature of the ionization also enables us to use the photoelectron peak positions to estimate the electronic origins of the 3s and $3p_x$ states (once again making use of the 8.20 eV D_0 adiabatic ionization potential). Values of 4.85 ± 0.03 eV (255.6 ±1.6 nm) and 5.65 ± 0.03 eV (219.4 ± 1.2 nm) are obtained, respectively. The former is good agreement with that quoted by Glendening and co-workers[19] from a room temperature vapour phase absorption measurement (258.3 nm, 4.80 eV), although the latter differs slightly to that reported by the same authors (226.9 nm, 5.46 eV).

A Levenberg-Marquardt global fitting routine was used to model the time-dependence of the 2D photoelectron data $S(E_B, \Delta t)$ using a total of 3 exponentially decaying functions – the minimum number required to achieve a satisfactory fit in this instance. Each function was

convoluted with the experimentally determined Gaussian cross-correlation $g(\Delta t)$ and set to originate from zero pump-probe delay, $\Delta t = 0$ (the significance of which will be expanded upon in the Discussion section).

$$S(E_B, \Delta t) = \left[\sum_{i=1}^{3} A_i(E_B) \exp\left(-\frac{\Delta t}{\tau_i} \right) \right] \otimes g(\Delta t) \quad (1)$$

The overall global fit to the data using the above expression is shown in the lower panel of Fig. 3. This approach also yields *decay associated spectra* (DAS) for each individual exponential function which plot the relative amplitudes A_i returned by the fit *vs* Rydberg binding energy E_B. We label each function using its respective decay constant $\tau_{1\text{-}3}$ and the corresponding DAS are shown in Fig. 5. The τ_1 DAS (60 ± 20 fs) describes an extremely rapid dynamical process that exhibits a very strong feature centred at 2.55 eV. There is also a negative amplitude component close to 3.35 eV. This coincides energetically with the strong positive amplitude peak present in the τ_2 DAS (180 ± 20 fs) which is superimposed on a broader background of lower amplitude spanning the 2.2-4.6 eV Rydberg binding energy region. A longer-lived dynamical feature described by the τ_3 DAS (1.7 ± 0.2 ps) also spans a similar binding energy region. This exhibits only a very small amplitude at all energies >2.2 eV but its inclusion was required to achieve a good quality fit. We note that the τ_1 and τ_2 values quoted here (60 and 180 fs) are in excellent agreement with time constants reported by Zhang and co-workers (62 fs and 184 fs) in their recent 400/800nm pump/probe TRPEI study of piperidine. In contrast to our work, however, these authors did not report a process associated with a third time constant.

C. Photoelectron Angular Distributions

Non-adiabatic coupling between different states effectively mixes their electronic (or vibronic) character. Temporal evolution of the photoelectron angular distributions (PADs)

observed in TRPEI measurements therefore provides a sensitive probe of this interaction.[33] TRPEI data obtained using (1 + 1′) ionization with parallel linear laser polarizations yields PADs with shapes described by the second- and fourth-order Legendre polynomials, weighted by the anisotropy parameters β_2 and β_4 – as discussed in detail elsewhere[34, 35] and employed extensively in our previous work.[1, 2, 16, 23, 36, 37] Fits to our piperidine PAD data reveal the evolution of β_2 and β_4 as a function of time, as shown in Fig. 6 for selected binding energy regions corresponding to the sharp peaks at 2.55 eV and 3.35 eV ($3p_x$ and 3s Rydberg ionization, respectively) and the broad feature extending to binding energies >3.5 eV. For the case of $3p_x$ ionization β_2 and β_4 both start at relatively high values (approximately 1.3 and 0.5, respectively) before falling in ~200 fs to a much lower plateau level. In contrast, ionization from the 3s Rydberg state results in an initial, very rapid rise in β_2 (to a value of approximately 0.7) followed by a fall on a more extended (~1 ps) timescale. Although the corresponding values obtained for β_4 are relatively small, it is also possible to make out a slight rise and fall in this parameter at early pump-probe delay times. A somewhat similar temporal evolution is also seen in the angular distribution associated with the broad spectral feature at Rydberg binding energies >3.5 eV although the overall anisotropy is greatly reduced in this case, with β_2 never exceeding a value of 0.2. The size of the β_2 and β_4 values exhibited by the sharp, intense peak at 2.55 eV ($3p_x$ ionization) are comparable to those reported recently in several tertiary amine systems,[1, 2] although for the weaker peak at 3.35 eV (3s ionization) they are somewhat lower. This is most likely a consequence of significant additional contributions to the overall anisotropy in this region from the broad, largely isotropic feature which extends underneath it. Considering the absolute magnitudes of the β_2 and β_4 parameters in more detail is not necessary for the dynamical interpretation presented in Section V and so is therefore beyond the scope of this present work. The reader is, however,

directed to our previous study on tertiary amine systems for a more expanded discussion of this aspect of the data.[1] Finally, the striking overall difference in the anisotropy exhibited by the sharp peaks at 2.55 eV and 3.35 eV when compared to the broader background is reinforced by the polar PAD plots shown in the lower section of Fig. 6, where the angular data is averaged over relevant energy regions close to zero pump-probe delay.

IV. THEORY

Supporting calculations investigating electronic state energies were performed using Gaussian09[38] and orbitals visualised using GaussView.[39] Ground state geometry optimization was performed using density functional theory (B3LYP)[40, 41] with the aug-cc-pVTZ basis set. As expected, the lowest energy piperidine structure was an equatorial chair conformation, with the axial chair form lying 278 cm^{-1} above this. Although this separation would not typically be resolvable in an ultrafast TRPEI measurement, it is sufficiently large that we may assume only the equatorial conformer is present to any significant extent in our experimental molecular beam. Even if this were not fully the case, however, we note that Ashfold and co-workers have reported that the equatorial and axial conformers of the related species morpholine exhibit identical photodissociation dynamics.[22] Vertical excitation energies and associated oscillator strengths (see Table I) were evaluated for the first four singlet excited states of piperidine (i.e. the 3s state and the x, y and z components of the 3p manifold) using equation of motion coupled cluster theory including single and double excitations (EOM-CCSD)[42] using the aug-cc-pVDZ basis. We note that previous benchmarking studies have demonstrated this choice of basis is well-suited to describing Rydberg states in similar molecules.[1] The character of each excited state is mixed between several Rydberg-type orbitals, but the principal component is always clearly identifiable (see the lower left panels of Fig. 7). Excitation at 200 nm (6.2 eV) will predominantly populate the $3p_x$ Rydberg state, which is the lowest lying member of the 3p manifold and carries by far the highest oscillator

strength (we use the standard Gaussian molecular orientation to define the axes). The predicted energy gap between the 3s and $3p_x$ Rydberg states is 0.77 eV. This agrees extremely well with the separation between the photoelectron peaks assigned to (diagonal) ionization from these states in our experimental data (0.80 eV). Based on the band origin positions extracted from the TRPEI data earlier (see section III. B), the calculations overestimate the absolute state energies by 0.56 eV. This is not an unexpected result, however, given that no additional corrections (i.e. zero-point energy, higher-order correlation, larger basis sets, core-valence correlation[43] etc.) have been applied to the calculation. The absolute error for the calculations employed here are consistent with benchmark calibrations on small to medium sized organic chromophores.[44, 45]

To investigate possible dissociative excited state relaxation channels, EOM-CCSD/aug-cc-pVDZ calculations were performed on piperidine to obtain potential energy curves along the N-H and N-C bonds. For reasons that will be expanded upon in the Discussion, curves were also evaluated for the D_0 state of the cation by relaxing the neutral geometries to those of the radical cation (with B3LYP/aug-cc-pVTZ), and then at each point performing subsequent N and N-1 electron CCSD/aug-cc-pVDZ energy differences to obtain the orbital relaxed ionization energies. As seen in the upper panels of Fig. 7, at extended N-C distances the $3p_x$ state appears to evolve a significant nσ* valence contribution while the 3s and higher-lying 3p states retain their predominantly Rydberg character. This leads to the 3s and $3p_x$ states becoming degenerate at ~ 1.9 Å. Along the N-H coordinate, however, the situation is different as now it is the 3s state that develops the nσ* character while all the 3p states remain Rydberg in nature. These differences in electronic character evolution along the two coordinates are also clearly seen in the representative orbital plots presented in the lower panels of Fig. 7. Our findings highlight that, although we have used the Rydberg character of the excited states as simple labels for identification and discussion purposes throughout, such

descriptions are only really valid in the vertical Franck-Condon region (i.e. when the excited state geometry is similar to that of the S_0 ground state). Over the full range of nuclear geometries that the system may sample following UV excitation, a more complete mixed Rydberg/valence picture of the excited states is clearly more appropriate. In the interests of clarity, the simple (e.g. 3s, $3p_x$) state labels will be largely retained throughout the remainder of this communication, although invoking the more complete mixed state description will prove essential in fully interpreting our TRPEI data in the following section.

V. DISCUSSION

A. Decay of the 3p State

As seen in Fig. 4, following 200 nm excitation the time-resolved photoelectron spectrum of piperidine displays two sharp, narrow peaks (at 2.55 eV and 3.35 eV) superimposed on a very broad background signal. The overall dynamical evolution of these features is extremely fast, with the system moving to a region of configuration space outside the experimental observation window in <2 ps (the longest-lived feature in Fig. 5 is the τ_3 DAS with an associated time constant of 1.7 ± 0.2 ps). As already discussion in Section III. C, the two sharp features may be assigned to ionization from states exhibiting $3p_x$ (2.55 eV) and 3s (3.35 eV) Rydberg character, respectively. From the energy level data and associated oscillator strengths presented in Table I, initial excitation at 200 nm will predominantly populate the $3p_x$ state, which is the lowest energy component of the 3p manifold. This then undergoes extremely rapid decay, as described by the τ_1 DAS (with an associated time-constant of 60 ± 20 fs). The τ_1 DAS also unambiguously reveals the fate of the $3p_x$ state population as the negative amplitude feature it exhibits at 3.35 eV coincides energetically with the strong positive amplitude peak present in the τ_2 DAS which is attributable to 3s ionization – strongly implying that internal conversion to this state is taking place. This illustrates an important advantage of the parallel fitting model described earlier, where all

exponential functions are set to originate from zero pump-probe delay: the negative amplitude in the τ_1 DAS close to 3.35 eV represents an exponential growth in photoelectron signals associated with the population of an electronic state that was not directly accessed in the initial excitation (i.e., a spectral feature that arises as a consequence of *sequential* dynamics – for example, via internal conversion). Although the parallel model may therefore not be a true physical representation of the dynamics, this choice of "basis" for extracting information has the advantage of assuming no *a priori* information about the nature (sequential or otherwise) of the various relaxation processes involved when fitting data. This is instead revealed by the fitting process itself. The negative signal in the τ_1 DAS can simply be viewed as a compensation effect, subtracting the positive amplitude at short delay times associated with a sequential feature in the experimental data (i.e., one not truly originating from zero pump-probe delay) described by the τ_2 DAS in the same energy region. Some instructive illustrative examples of this effect may be found in the work of Stolow and co-workers.[46] Further evidence of the $3p_x/3s$ internal conversion is also seen in the PAD anisotropy data presented in Fig. 6, where the evolution of both β_2 and β_4 on timescales mirroring the DAS time constants provides strong additional signatures of the non-adiabatic coupling process. More detailed (i.e. fully quantitative) analysis of this aspect of our data is challenging, however, due to additional dynamical factors that may influence/convolute the observed PADs. These include changes in the relative amplitudes and phases of the outgoing photoelectron partial waves due to structural changes influencing the scattering dynamics off the non-spherical ion core potential and variations in excited state Rydberg vs. valance character as a function of certain nuclear coordinates. Any loss of Rydberg character is a different effect to changes in electronic character induced by state mixing interactions – as has been considered in detail elsewhere.[47]

In order for $3p_x/3s$ internal conversion to occur via a conical intersection, the two states must reach a point of electronic degeneracy. On the basis of the calculations presented in Fig. 7, a critical nuclear motion required to facilitate this process is along the N-C stretch co-ordinate, where the $3p_x$ state evolves significant nσ* valence character and crosses the 3s surface at ~1.9 Å. Such observations are consistent with findings reported previously for several tertiary aliphatic amine systems[1, 2], which have also provided strong experimental and theoretical evidence to suggest that planarity about the N atom is *not* a prerequisite for this specific internal conversion process to occur.

B. Decay of the 3s State

Once population has transferred non-adiabatically to the 3s state, a second ultrafast decay is then observed, as modelled by the τ_2 DAS in Fig. 5 (exhibiting a time-constant of 180 ± 20 fs). The ionization signal associated with this process appears to have two distinct components, as is evident from the very different photoelectron anisotropy seen in the narrow feature at close to 3.35 eV and the much broader feature that extends underneath it (Fig. 6). As discussed in Section IV, the use of simple Rydberg-type labels to describe the electronic states of piperidine is not always a fully accurate description. For those states in which significant nσ* valence character develops as certain nuclear coordinates are extended, such labels are only valid in the vertical Franck-Condon region. A more complete, mixed Rydberg/valence picture will therefore be more instructive in interpreting the spectral signatures of the excited state dynamics observed in our data. As seen in Fig. 7(b), following internal conversion the excited state vibrational wavepacket will encounter a bound potential along the N-C coordinate of the 3s state. This results in the system rapidly moving back towards the Franck-Condon region before freely extending again along the N-H coordinate of the 3s state towards an asymptotic dissociation limit, ultimately yielding H atom photoproducts (expanded upon in more detail shortly). In undergoing this evolution, the

system will therefore sample a wide range of nuclear geometries where the electronic state character changes rapidly from Rydberg to valence character on the 3s potential surface – see Fig. 7. This H atom motion will occur extremely rapidly and is not expected to be temporally resolvable in our experiments (given the instrument response function of 160 fs). However, we suggest that our data does appear to reflect this evolution in a *spectrally averaged* way since the increased nσ* valence character developed at extended N⁻H distances then leads to a reduction in the propensity for diagonal ionisation, resulting in a much broader feature in the photoelectron spectra/τ_2 DAS (see Figs 4 & 5). An associated reduction in the anisotropy parameters associated with this ionization signal would also be expected (as is readily seen in the lowest panel of Fig. 6) due to the angular momentum of the increased valence character contribution being much less well-defined than for the Rydberg component (i.e. the state is no longer described predominantly by a single s-type basis orbital). These nσ* signals are convoluted with the narrow, anisotropic peak at 3.35 eV that provides a signature of 3s Rydberg character ionization from the same state within the vertical Franck-Condon region. We note that the same arguments have previously been suggested to explain very similar (although more spectrally obscured) dynamical features present in TRPEI data obtained from aniline and some of its methyl-substituted derivatives.[16, 48-50] We also suggest that the τ_1 DAS in Fig. 4 (associated with the decay of the initially prepared $3p_x$ state) also reflects a similar spectrally averaged Rydberg-to-valence evolution as it exhibits small non-zero amplitude over a range of binding energies >4.0 eV. Further support for this assertion is also indicated in the relative size of the positive and negative peaks seen at 3.35 eV in the τ_2 and τ_1 DAS, respectively, as the latter is smaller in amplitude. Assuming negligible direct optical excitation to the 3s state at 200 nm (which is reasonable, given the absorption spectrum in Fig. 1 and the calculated oscillator strengths in Table I), this discrepancy may therefore be

attributed to a broad, weak underlying feature in the τ_1 DAS extending all the way to the strong peak at 2.55 eV.

More generally, we anticipate that the distinct spectral signatures described above should be generally observable in TRPEI measurements conducted on a wide range of molecular systems where ionization efficiently samples a state of mixed Rydberg/valance character evolving over a large range of bond extensions. This does, however, come with two important caveats: (i) in instances where the potential energy surface of the cation exhibits markedly different topology to that of the state being ionized, Frank-Condon considerations may mean the effective observation window of the experiment may be too limited to fully reflect the evolution of the orbital character; (ii) although the sharp and highly anisotropic ionization signatures associated with the Rydberg component provide a particularly useful marker for identification, such features may not always be observed in situations where a mixed Rydberg/valence character state is only populated indirectly via non-adiabatic processes (i.e. at extended coordinate distances where the valence character is dominant) – especially if the system is then subsequently unable to return to the Franck-Condon geometry, as suggested in our recent work on indole.[36] With regard to point (i) we note that in our present experiments the total pump + probe energy (10.85 eV) greatly exceeds the piperidine D_0 ionization potential (8.20 eV). Although the 3s/nσ* and D_0 potential surfaces are very different along the N-H stretch (see Fig. 7), the fact that we may project up to 2.65 eV above the D_0 cation origin provides a very favourable window of observation along this particular reaction coordinate, permitting good (spectral) resolution of the Rydberg-to-valence evolution in this instance.

Having assigned the τ_2 DAS to extremely rapid 3s to nσ* evolution along the N-H stretching coordinate, the origin of the spectral signature giving rise to the small-amplitude τ_3 DAS (with associated time-constant of 1.7 ± 0.2 ps) initially seems less clear. As noted in the

Introduction, however, Ashfold and co-workers have previously reported two distinct H atom kinetic energy release channels in the structurally related species morpholine following UV excitation over the 250-193 nm excitation region.[22] These are attributed to subsets of dissociating molecules that exhibit either planar geometries about the N atom centre upon first encountering an $n\sigma^*/S_0$ conical intersection at highly extended N-H distances (and so rapidly pass straight through it) or are non-planar at this point and so undergo a more "frustrated" process, repeatedly resampling the conical intersection until the correct region of phase space is achieved. Similar conclusions have also been drawn to explain related experimental observations in the ammonia[3, 6, 51, 52], methylamine[53] and 3-pyrroline[54] systems. We therefore suggest that the same dynamics operate here in piperidine: dissociation leading to H atom photoproducts from the S_0 ground state may occur either promptly upon an initial encounter with the $n\sigma^*/S_0$ conical intersection (as described by the τ_2 DAS) or via the longer-time process where excited state population remains effectively trapped at extended N-H distances on the $n\sigma^*$ potential surface for a more extended period before population transfer to S_0 takes place (described by the τ_3 DAS). Following 200 nm excitation we also highlight that it is likely the dissociation channel leading to H atom formation in conjunction with excited ($\tilde{A}$) state piperidinyl fragments should, in principle, also be accessible – produced via direct dissociation on the (adiabatic) $3s/n\sigma^*$ potential surface. It is, however, interesting to note that (when energetically open) this channel has not been conclusively observed in systems other than ammonia, although the specific reason for this appears to be an open question.[54] Overall, our data therefore appear to provide a detailed time-resolved picture of the relaxation dynamics operating in piperidine that is consistent with previous studies employed on closely related systems exploiting a range of experimental approaches (with different associated observables). In particular, the relatively low ionization potential of piperidine compared to

the total pump + probe energy offers a considerable advantage in following the dynamics out to extended N-H bond distances. The highly-differential time- and energy-resolved information afforded by the TRPEI approach offers considerable mechanistic insight overall and also serves to highlight key differences between the UV-induced relaxation processes operating in primary/secondary aliphatic amines and the tertiary systems we have investigated previously. Building on these initial findings, we aim to continue our systematic investigations of amine photophysics in the near future.

VI. CONCLUSION

Electronic relaxation dynamics in the alicyclic secondary amine piperidine were investigated following 200 nm excitation using the time-resolved photoelectron imaging (TRPEI) technique. On the basis of our experimental data, supported by quantum-chemistry calculations, we have gained considerable insight into the non-adiabatic couplings that facilitate the dissipation of excess energy in this system. Initial absorption is predominantly to the lowest-lying member of the 3p Rydberg manifold ($3p_x$) which then undergoes extremely rapid (60 fs) internal conversion to a new electronic state exhibiting 3s Rydberg character in the vertical Franck-Condon region. A critical nuclear motion required to initiate this process is extension along the N-C stretching coordinate, during which the $3p_x$ state evolves $n\sigma^*$ valence character. Once populated, the 3s state is then able to dissociate to yield H atom photoproducts and in doing so samples a range of N-H bond extensions over which, once again, significant $n\sigma^*$ valence character develops. This leads to a distinct, rapidly decaying spectral signature in the TRPEI data consisting of a sharp and highly anisotropic photoelectron signal (3s Rydberg-type ionization from the Franck-Condon region) superimposed on a much broader and largely isotropic feature ($n\sigma^*$ valence character ionization at more extended N-H distances). Temporal resolution of this process is not possible in our current experiments but it is, instead, seen in a spectrally averaged manner.

Finally, at even more extended N-H distances population on the 3s potential energy surface (which should more formally be described as nσ* outside the Franck-Condon region) may move through a conical intersection with the S_0 state to ultimately yield H atom photoproducts in conjunction with ground state piperidinyl radicals. Piperidine molecules encountering this conical intersection with planar geometries about the N atom centre will undergo this process extremely rapidly (180 fs) whereas those exhibiting non-planar geometries at this point will repeatedly resample the CI until the correct structure is assumed, ultimately dissociating on a more extended (1.7 ps) timescale. Overall, our findings reveal the role played by multiple nuclear coordinate motions in driving stepwise internal conversion across several different potential energy surfaces and also highlight the distinct photoionization signatures that are associated with these processes. We anticipate that such signatures will be generally observable for a wide range of molecular systems exhibiting states of mixed Rydberg/valence character, and hope that our present findings may therefore serve as a useful aid to their spectroscopic assignment.

ACKNOWLEDGEMENTS

This work was made possible by financial support from EPSRC Grant No. EP/G041717/1. LBK thanks the Danish Council for Independent Research | Natural Sciences (FNU) for PhD funding, and the Oticon Foundation and Augustinus Foundation for travel stipends. JOFT and SWC thank Heriot-Watt University for PhD funding. The European Research Council supports MJP under the European Union's Seventh Framework Programme (FP7/2007–2013)/ERC Grant No. 258990. Associated data are deposited with the Heriot-Watt Research Archive.

REFERENCES

1. J. O. F. Thompson, L. B. Klein, T. I. Sølling, M. J. Paterson and D. Townsend, *Chem. Sci.*, 2016, **7**, 1826.
2. L. B. Klein, T. J. Morsing, R. A. Livingstone, D. Townsend and T. I. Sølling, *Phys. Chem. Chem. Phys.*, 2016, **18**, 9715.
3. M. N. R. Ashfold, G. A. King, D. Murdock, M. G. D. Nix, T. A. A. Oliver and A. G. Sage, *Phys. Chem. Chem. Phys.*, 2010, **12**, 1218.
4. G. M. Roberts and V. G. Stavros, *Chem. Sci.*, 2014, **5**, 1698.
5. N. L. Evans, H. Yu, G. M. Roberts, V. G. Stavros and S. Ullrich, *Phys. Chem. Chem. Phys.*, 2012, **14**, 10401.
6. H. Yu, N. L. Evans, A. S. Chatterley, G. M. Roberts, V. G. Stavros and S. Ullrich, *J. Phys. Chem. A*, 2014, **118**, 9438.
7. K. L. Wells, G. Perriam and V. G. Stavros, *J. Chem. Phys.*, 2009, **130**, 074308.
8. E. Kassab and E. M. Evleth, in *The Role of Rydberg States in Spectroscopy and Photochemistry*, ed. C. Sándorfy, Kluwer Academic Publishers, Hingham, MA, USA, 1999, p. 231.
9. R. Marom, C. Levi, T. Weiss, S. Rosenwaks, Y. Zeiri, R. Kosloff and I. Bar, *J. Phys. Chem. A*, 2010, **114**, 9623.
10. N. R. Forde, M. L. Morton, S. L. Curry, S. J. Wrenn and L. J. Butler, *J. Chem. Phys.*, 1999, **111**, 4558.
11. J. D. Cardoza, F. M. Rudakov and P. M. Weber, *J. Phys. Chem. A*, 2008, **112**, 10736.
12. S. Deb, B. A. Bayes, M. P. Minitti and P. M. Weber, *J. Phys. Chem. A*, 2011, **115**, 1804.
13. J. C. Bush, M. P. Minitti and P. M. Weber, *J. Phys. Chem. A*, 2010, **114**, 11078.
14. M. P. Minitti and P. M. Weber, *Phys. Rev. Lett.*, 2007, **98**, 253004.
15. J. L. Gosselin, M. P. Minitti, F. M. Rudakov, T. I. Sølling and P. M. Weber, *J. Phys. Chem. A*, 2006, **110**, 4251.
16. J. O. F. Thompson, L. Saalbach, S. W. Crane, M. J. Paterson and D. Townsend, *J. Chem. Phys.*, 2015, **142**, 114309.
17. X. Qiu, J. Long, Z. Liu and B. Zhang, *Chem. Phys. Lett.*, 2016, **645**, 133.
18. T. Streibel, K. Hafner, F. Mühlberger, T. Adam and R. Zimmerman, *Appl. Spectrosc.*, 2006, **60**, 72.
19. A. M. Halpern, B. R. Ramachandran and E. D. Glendening, *J. Phys. Chem. A*, 2000, **104**, 11733.
20. S. Nath, R. S. Singh and G. D. Baruah, *Indian J. Pure Appl. Phys.*, 1972, **10**, 490.
21. L. W. Pickett, M. E. Corning, G. M. Wieder, D. A. Semenow and J. M. Buckley, *J. Am. Chem. Soc.*, 1953, **75**, 1618.
22. T. A. A. Oliver, G. A. King and M. N. R. Ashfold, *Chem. Sci.*, 2010, **1**, 89.
23. R. A. Livingstone, J. O. F. Thompson, M. Iljina, R. J. Donaldson, B. Sussman, M. J. Paterson and D. Townsend, *J. Chem. Phys.*, 2012, **137**, 184304.
24. U. Even, J. Jortner, D. Noy, N. Lavie and C. Cossart-Magos, *J. Chem. Phys.*, 2000, **112**, 8068.
25. A. T. J. B. Eppink and D. H. Parker, *Rev. Sci. Instrum.*, 1997, **68**, 3477.
26. E. Tannenbaum, E. M. Coffin and A. J. Harrison, *J. Chem. Phys.*, 1953, **21**, 311.
27. M. B. Robin, *Higher Excited States of Polyatomic Molecules I*, Academic Press, New York, 1974.
28. M.-J. Hubin-Franskin, J. Delwiche, F. Tollet, M. Furlan and J. E. Collin, *J. Phys. B: At. Mol. Opt. Phys.*, 1988, **21**, 189.

29. P. Avouris and A. R. Rossi, *J. Phys. Chem.*, 1981, **85**, 2340.
30. A. Osted, J. Kongsted and O. Christiansen, *J. Phys. Chem. A*, 2005, **109**, 1430.
31. M. D. Rozeboom and K. N. Houk, *J. Am. Chem. Soc.*, 1982, **104**, 1189.
32. T.-H. Gan and J. B. Peel, *Aust. J. Chem.*, 1979, **32**, 475.
33. G. Wu, P. Hockett and A. Stolow, *Phys. Chem. Chem. Phys.*, 2011, **13**, 18447.
34. K. L. Reid, *Annu. Rev. Phys. Chem.*, 2003, **54**, 397.
35. T. Suzuki, *Annu. Rev. Phys. Chem.*, 2006, **57**, 555.
36. M. M. Zawadzki, J. O. F. Thompson, E. A. Burgess, M. J. Paterson and D. Townsend, *Phys. Chem. Chem. Phys.*, 2015, **17**, 26659.
37. J. O. F. Thompson, R. A. Livingstone and D. Townsend, *J. Chem. Phys.*, 2013, **139**, 034316.
38. M. J. Frisch, G. W. Trucks, H. B. Schlegel, G. E. Scuseria, M. A. Robb, J. R. Cheeseman, G. Scalmani, V. Barone, B. Mennucci, G. A. Petersson, H. Nakatsuji, M. Caricato, X. Li, H. P. Hratchian, A. F. Izmaylov, J. Bloino, G. Zheng, J. L. Sonnenberg, M. Hada, M. Ehara, K. Toyota, R. Fukuda, J. Hasegawa, M. Ishida, T. Nakajima, Y. Honda, O. Kitao, H. Nakai, T. Vreven, J. J. A. Montgomery, J. E. Peralta, F. Ogliaro, M. Bearpark, J. J. Heyd, E. Brothers, K. N. Kudin, V. N. Staroverov, R. Kobayashi, J. Normand, K. Raghavachari, A. Rendell, J. C. Burant, S. S. Iyengar, J. Tomasi, M. Cossi, N. Rega, J. M. Millam, M. Klene, J. E. Knox, J. B. Cross, V. Bakken, C. Adamo, J. Jaramillo, R. Gomperts, R. E. Stratmann, O. Yazyev, A. J. Austin, R. Cammi, C. Pomelli, J. W. Ochterski, R. L. Martin, K. Morokuma, V. G. Zakrzewski, G. A. Voth, P. Salvador, J. J. Dannenberg, S. Dapprich, A. D. Daniels, Ö. Farkas, J. B. Foresman, J. V. Ortiz, J. Cioslowski and D. J. Fox, Gaussian, Inc., Wallingford CT2009.
39. R. Dennington, T. Keith and J. Millam, Semichem Inc., Shawnee Mission, KS2009.
40. P. J. Stephens, F. J. Devlin, C. F. Chabalowski and M. J. Frisch, *J. Phys. Chem.*, 1994, **98**, 11623.
41. A. D. Becke, *J. Chem. Phys.*, 1993, **98**, 5648.
42. H. Koch and P. Jørgensen, *J. Chem. Phys.*, 1990, **93**, 3333.
43. D. J. Taylor and M. J. Paterson, *J. Chem. Phys.*, 2010, **133**, 204302.
44. M. Schreiber, M. R. Silva-Junior, S. P. A. Sauer and W. Thiel, *J. Chem. Phys.*, 2008, **128**, 134110.
45. M. R. Silva-Junior, S. P. A. Sauer, M. Schreiber and W. Thiel, *Mol. Phys.*, 2010, **108**, 453.
46. O. Schalk, A. E. Boguslavskiy and A. Stolow, *J. Phys. Chem. A*, 2010, **114**, 4058.
47. M. Rubio, L. Serrano-Andrés and M. Merchán, *J. Chem. Phys.*, 2008, **128**, 104305.
48. O. M. Kirkby, M. Sala, G. Balerdi, R. de Nalda, L. Bañares, S. Guérin and H. H. Fielding, *Phys. Chem. Chem. Phys.*, 2015, **17**, 16270.
49. R. Spesyvtsev, O. M. Kirkby, M. Vacher and H. H. Fielding, *Phys. Chem. Chem. Phys.*, 2012, **14**, 9942.
50. R. Spesyvtsev, O. M. Kirkby and H. H. Fielding, *Faraday Discuss.*, 2012, **157**, 165.
51. A. S. Chatterley, G. M. Roberts and V. G. Stavros, *J. Chem. Phys.*, 2013, **139**, 034318.
52. J. D. Rodríguez, M. G. González, L. Rubio-Lago and L. Bañares, *Phys. Chem. Chem. Phys.*, 2014, **16**, 406.
53. C. L. Reed, M. Kono and M. N. R. Ashfold, *J. Chem. Soc., Faraday Trans.*, 1996, **92**, 4897.
54. T. A. A. Oliver, G. A. King and M. N. R. Ashfold, *J. Chem. Phys.*, 2010, **133**, 194303.

TABLE CAPTIONS

Table I. Unrelaxed EOM-CCSD/aug-cc-pVDZ vertical excitation energies (*E*) and oscillator strengths (*f*) for piperidine evaluated using the global energy minimum ground state structure optimized at the B3LYP/aug-cc-pVTZ level. Labelling of the *x*, *y* and *z* axes for the 3p states follows standard Gaussian09 conventions.

Table I

	$3s \leftarrow n$	$3p_x \leftarrow n$	$3p_z \leftarrow n$	$3p_y \leftarrow n$
E/eV	5.41	6.18	6.30	6.36
f	0.001	0.085	0.010	0.011

FIGURE CAPTIONS

Figure 1. UV vapour-phase room temperature absorption spectrum of piperidine (a schematic structure of which is inset) recorded using a commercial bench-top spectrophotometer (Camspec M550).

Figure 2. (1 + 1′) photoelectron images from piperidine obtained at selected pump-probe delay times using a 200 nm pump/267 nm probe. Time-invariant pump-alone and probe-alone signals have been subtracted and the images are 4-fold symmetrised. The left half of each image shows the result following application of a rapid matrix inversion approach (required for generation of the time-resolved photoelectron spectra in Figs 3 & 4), as described in detail in Ref. 23. The (linear) polarization direction of the pump and probe beams is vertical with respect to the figure.

Figure 3. 3D time-dependent photoelectron spectrum of piperidine obtained using a 200 nm pump/267 nm probe (top), and corresponding fit to the data (bottom – see main text for more details). For clear display of the dynamics over all temporal ranges, the time axis is linear to +1 ps and then logarithmic beyond this point.

Figure 4. 2D time-dependent photoelectron spectra of piperidine obtained using a 200 nm pump/267 nm probe. As in Fig. 3, the time axis is linear to +1 ps and then logarithmic beyond this point. The intensity colour map is presented on a natural logarithmic scale based on the output directly obtained from the imaging CCD camera.

Figure 5. Decay associated spectra (DAS) obtained from the global exponential fit detailed in the main text. The uncertainties quoted are 1σ values and the data is partitioned into 0.025 eV energy bins.

Figure 6. Upper panels: Evolution of the anisotropy parameters β_2 and β_4 vs. pump–probe delay following 200 nm pump/267 nm probe ionization of piperidine. Plots show values averaged over the energy regions highlighted using the vertical dashed white lines on the inset

2D spectra. Within each selected energy region, the β_2 and β_4 values (and associated temporal changes) are broadly consistent and averaging only serves to improve the signal-to-noise. The time axis is linear to +1 ps and then logarithmic to +10 ps. The data was partitioned into 0.025 eV energy bins for the initial anisotropy fits (before averaging) and the error bars denote 1σ values. Fits were performed over the angular region $10^{\circ} \leq \theta \leq 90^{\circ}$ to eliminate uncertainties from centre-line noise present in the Abel-inverted images (see Fig. 2). The grey line is the (intensity normalised) photoelectron signal averaged within the same energy region. Lower panels: Normalized polar PAD plots showing the angular data averaged over the same energy regions close to zero pump-probe delay (0-100 fs for the 3p state, 50-150 fs for 3s/nσ*). The red solid lines are the corresponding fits to the data obtained using $I(\theta) \propto \left[1 + \beta_2 P_2(\cos\theta) + \beta_4 P_4(\cos\theta)\right]$. Here the $P_n(\cos\theta)$ terms are the second- and fourth-order Legendre polynomials. The β_2 and β_4 anisotropy parameters obtained from these fits are also shown and the values in parentheses denote 1σ uncertainties in the final significant figure.

Figure 7. Upper panels: EOM-CCSD/aug-cc-pVDZ potential energy cuts for piperidine along the N-H and N-C stretching coordinates for the S_0, 3s, 3p and D_0 states. Lower panels: largest orbital transition in the EOM-CCSD eigenvectors at extended distances along the N-H (1.6 Å) and N-C (2.2 Å) coordinates within the excited states. Boxes highlighted in red indicate instances where a significant nσ* valence contribution is present. All orbital surfaces are plotted using the same iso values (0.15).

Figure 1

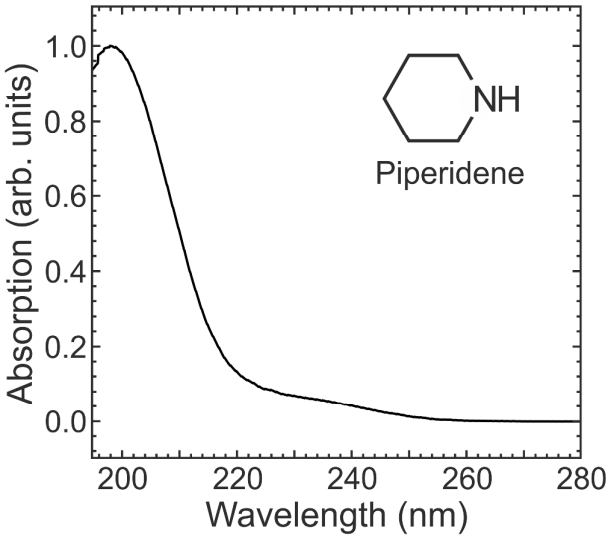
Absorption (arb. units)
1.0
0.8
0.6
0.4
0.2
0.0
200
220
240
260
280
Wavelength (nm)
NH
Piperidene

Figure 2

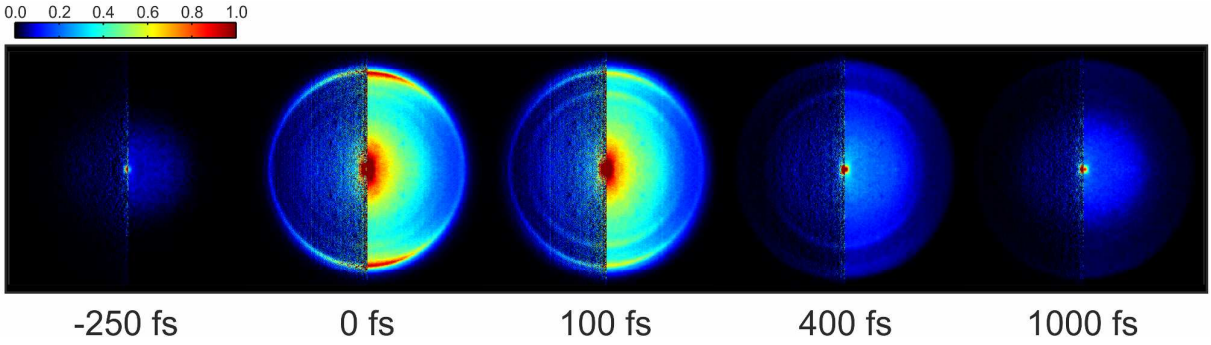

Figure 3

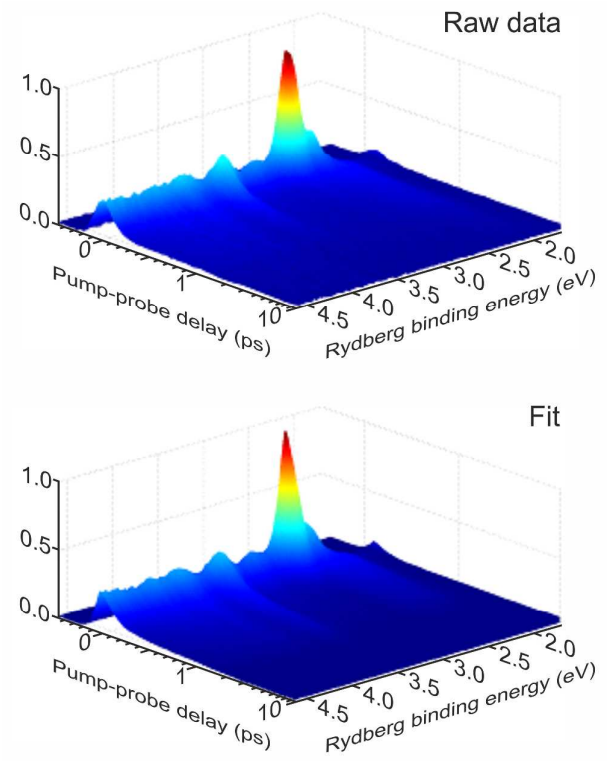
Raw data
1.0
0.5
0.0
0
1
10
Pump-probe delay (ps)
4.5
4.0
3.5
3.0
2.5
2.0
Rydberg binding energy (eV)
Fit
1.0
0.5
0.0
0
1
10
Pump-probe delay (ps)
4.5
4.0
3.5
3.0
2.5
2.0
Rydberg binding energy (eV)

Figure 4

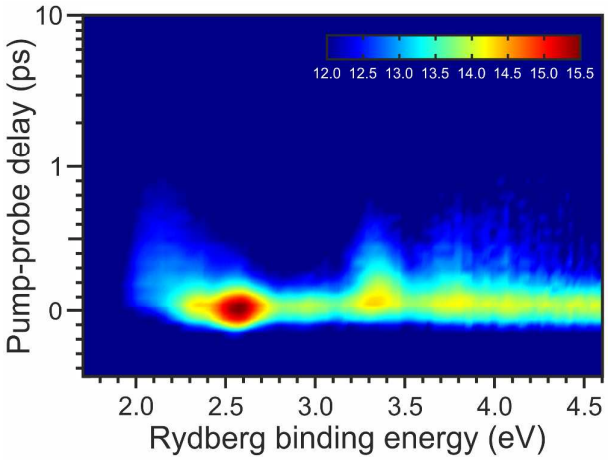
10
1
0
Pump-probe delay (ps)
12.0 12.5 13.0 13.5 14.0 14.5 15.0 15.5
2.0 2.5 3.0 3.5 4.0 4.5
Rydberg binding energy (eV)

Figure 5

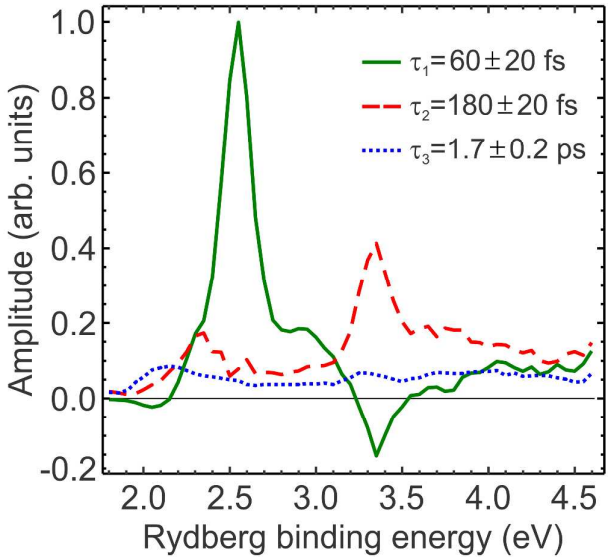
1.0
0.8
0.6
0.4
0.2
0.0
-0.2
Amplitude (arb. units)
2.0
2.5
3.0
3.5
4.0
4.5
Rydberg binding energy (eV)
τ1=60±20 fs
τ2=180±20 fs
τ3=1.7±0.2 ps

Figure 6

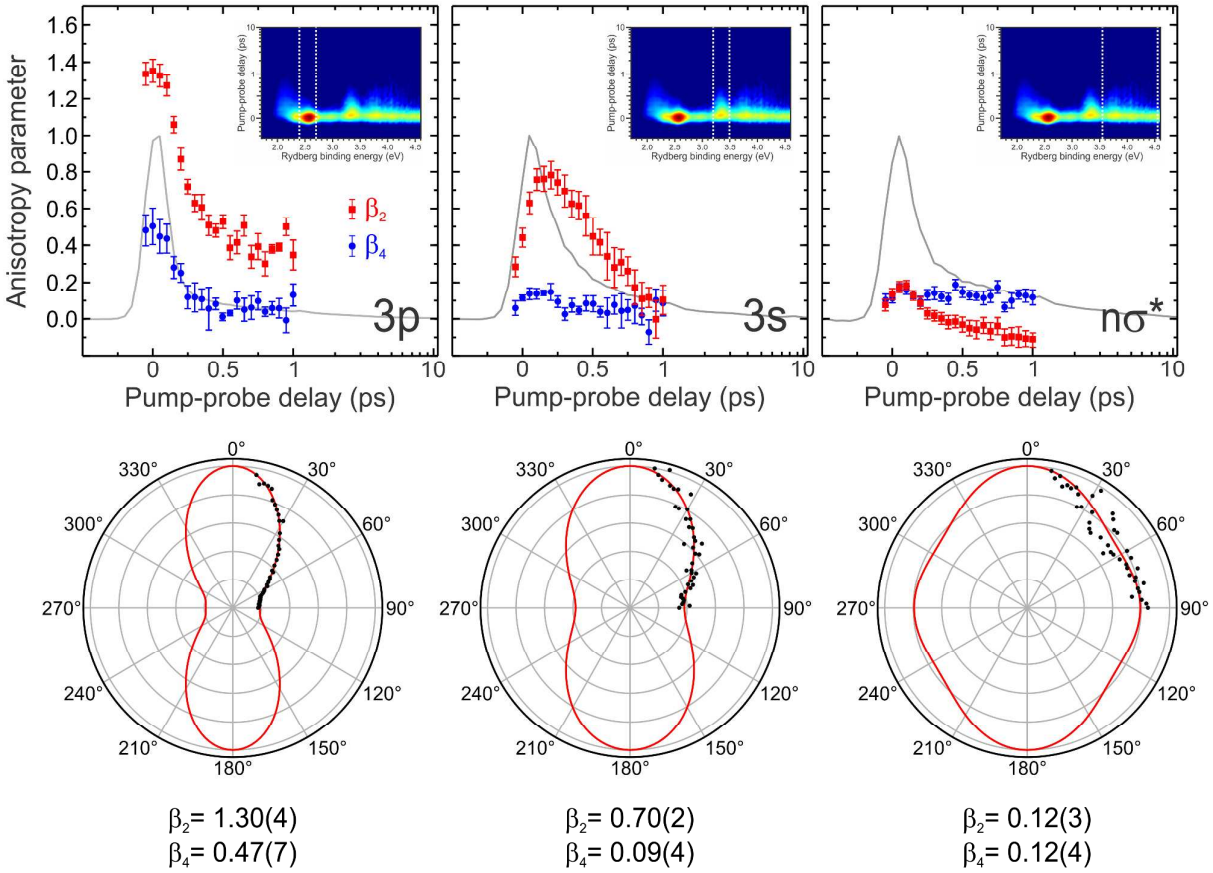
Anisotropy parameter
Pump-probe delay (ps)
Rydberg binding energy (eV)
β2
β4
3p
3s
nσ*
β2= 1.30(4)
β4= 0.47(7)
β2= 0.70(2)
β4= 0.09(4)
β2= 0.12(3)
β4= 0.12(4)

Figure 7

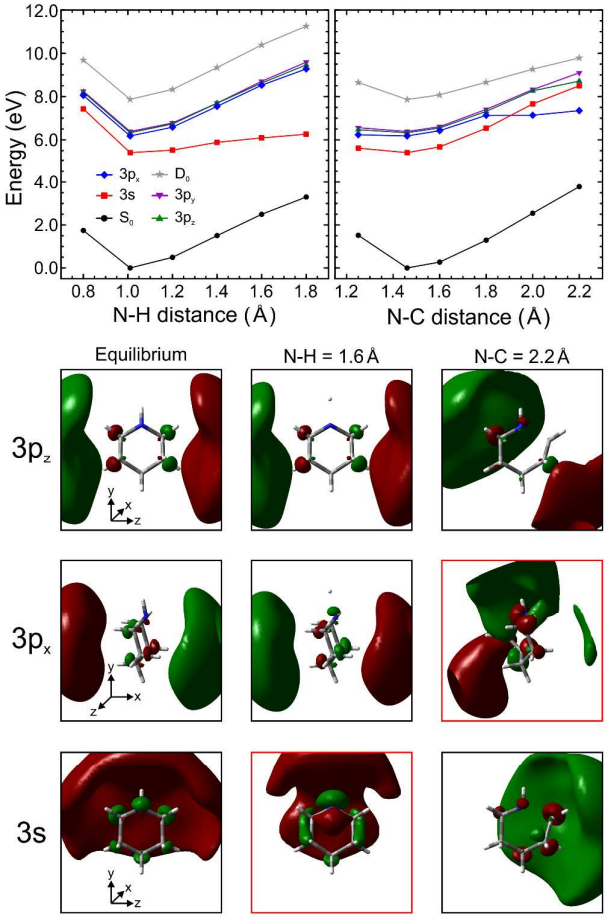
Energy (eV)
N-H distance (Å)
N-C distance (Å)
3p$_x$
D$_0$
3s
3p$_y$
S$_0$
3p$_z$
Equilibrium
N-H = 1.6 Å
N-C = 2.2 Å
3p$_z$
3p$_x$
3s